62 72411 Copy 462

[redacted] NASA TM X-587

NASA TM X-587

CLASSIFICATION CHANGED
UNCLASSIFIED
TO.....
By Authority FD-70-617 10/5/71

TECHNICAL MEMORANDUM

X-587 Declassified by authority of NASA
Classification Change Notices No. 212
Dated **12/31/71

INVESTIGATION OF FLUTTER CHARACTERISTICS OF FOUR SERIES OF LOW-ASPECT-RATIO SURFACES AT MACH NUMBERS FROM 1.49 TO 2.87

By Robert V. Doggett, Jr., and John G. Presnell, Jr.

Langley Research Center
Langley Field, Va.

[redacted]

[redacted]

NATIONAL AERONAUTICS AND SPACE ADMINISTRATION

WASHINGTON [redacted] September 1961

[redacted]

J

[redacted]

NATIONAL AERONAUTICS AND SPACE ADMINISTRATION

TECHNICAL MEMORANDUM X-587

INVESTIGATION OF FLUTTER CHARACTERISTICS OF FOUR SERIES OF LOW-ASPECT-RATIO SURFACES AT MACH NUMBERS FROM 1.49 TO 2.87*

By Robert V. Doggett, Jr., and John G. Presnell, Jr.

SUMMARY

Wind-tunnel tests have been completed on four series of low-aspect-ratio surfaces in the Mach number range from 1.49 to 2.87. Three of the series tested consisted of a cantilevered inboard panel with a tip control surface forming the outboard portion of the configuration. The fourth series consisted of sting-mounted matched pairs of all-movable control surfaces linked through a spring simulating the stiffness of a common actuator system. Models of each series with several different values of the ratio of uncoupled bending frequency to uncoupled rotational frequency were tested. Some of the models tested were equipped with mass balance. Within the range covered, it was found that the lowest flutter dynamic pressures were obtained when the ratio of uncoupled bending frequency to uncoupled rotational frequency was near 1 and that flutter may be eliminated or the dynamic pressure at flutter may be increased by the use of mass balance, the effect being greater at the lower frequency ratios.

Calculations based on piston theory gave good results for all models of one of the series with the movable surface forming the outboard portion. Similar calculations for the other two series with the tip control surface were highly unconservative. The reason for this unconservatism was not determined.

INTRODUCTION

Aeroelastic instabilities such as flutter and divergence have for years been problems faced by the designers of aircraft. It appears that such problems will continue to be quite critical. Indeed, the use of

[redacted]

[redacted]

aerodynamic surfaces for stability and control on missiles operating within the earth's atmosphere (such as ground-to-air, air-to-ground, and air-to-air missiles) has increased the general overall area where aeroelastic problems are of concern. There is some information available from wind-tunnel tests on surfaces suitable for use on missiles (see, for example, ref. 1), but extensive data on a variety of configurations is lacking. In the absence of proven analytical methods to fill the void left by the limited experimental results available, proposed aerodynamic surfaces must usually be tested for flutter.

Consequently, a series of 1/4-scale models of the aerodynamic surfaces of a ground-to-air missile were constructed and have been tested in the Langley Unitary Plan wind tunnel over the Mach number range from 1.49 to 2.87. Four different series of models were tested. Three of the configurations consisted of a cantilevered inboard panel with a tip control surface forming the outboard portion of the configuration. The fourth configuration was a sting-mounted matched pair of all-movable control surfaces linked through a spring simulating the stiffness of a common actuator system. The effects of variations of frequency ratio - ratio of uncoupled bending to uncoupled control rotation - on the flutter characteristics of all configurations were investigated. Also, studies were made of the effects of mass balance as a flutter alleviator.

Some of the experimental results were compared with calculated results. The analytical treatment used was of the Rayleigh type, using two uncoupled modes and second-order piston theory aerodynamics.

SYMBOLS

b	reference length, $\bar{c}/2$
c	chord
$\bar{c}$	mean aerodynamic chord
g	structural damping coefficient
I_{α}	mass moment of inertia about center of gravity
l	span
M	Mach number
m	mass

q	dynamic pressure, $\frac{1}{2}\rho V^2$
V	stream velocity
x	distance from trailing edge to center of gravity, measured parallel to root chord
y	distance from root chord to center of gravity, measured perpendicular to root chord
ρ	density
ω	circular frequency
μ	mass-ratio parameter, $\dfrac{m}{\int_0^l \rho\pi\left(\frac{c}{2}\right)^2 dy}$

Subscripts:

c	calculated
f	values at flutter
h	bending mode
α	torsional mode
β	antisymmetrical rotational mode
θ	rotational mode

APPARATUS AND PROCEDURE

Wind Tunnel

The investigation was conducted in the low Mach number test section of the Langley Unitary Plan wind tunnel. This tunnel is a variable-pressure, continuous, return-flow type. The test section is 4 feet square and approximately 7 feet in length. The nozzle leading to the test section is of the asymmetric sliding-block type. The Mach number can be varied continuously through a range from approximately 1.49 to 2.87.

Models

Configuration.- Four series of models were tested. The models of three of the series consisted of a cantilevered inboard panel with a tip control surface forming the outboard portion. The models of the fourth series were sting-mounted matched pairs of all-movable surfaces, linked through a spring simulating the stiffness of a common actuator system. Drawings of the models, giving the details of model geometry, are presented in figure 1. All models tested had circular-arc airfoil sections, modified over the truncated portion of the planforms to have a blunt trailing edge.

The models of series 1 had a panel aspect ratio of 1.12, a leading-edge sweep of 50°, a thickness-chord ratio of 5 percent, and were equipped with a tip control surface attached to a cantilevered inboard panel through a hinge tube located at 36.6 percent of the mean aerodynamic chord. The surface area of the control surface was 21.5 percent of the total planform area. The main configuration variable within this series was the rotational stiffness of the movable surface. This stiffness was controlled by varying the stiffness of a cantilever spring which restrained the hinge tube in rotation. Two models of this series were tested with a boom-mounted mass balance attached to the movable surface. This boom was attached at the 81.5-percent-span station and increased the weight of the basic movable surface by about 18 percent. The addition of the boom produced a forward shift of the control-surface center of gravity of about 2.7 percent of the mean aerodynamic chord. The models of this series were mounted on the tunnel sidewall. In order to minimize boundary-layer effects the models were attached to a fixed strut extending about 4 inches from the tunnel wall. The main spar of the model was rigidly attached to the strut and the model was pinned to the strut near the leading edge to prevent any twisting of the spar at the model root. This method of mounting was similar to that employed on the full-scale missile. A photograph of a typical model of this series mounted in the test section is shown as figure 2(a).

The models of both series 2 and 3 had a panel aspect ratio of 1.19, a leading-edge sweep of 31.66°, a thickness-chord ratio of 5.75 percent, and were equipped with a tip control surface attached to a cantilevered inboard panel through a hinge tube located at 49 percent of the mean aerodynamic chord. The surface area of the control surface was 28.8 percent of the total planform area. The differences between the two series were in the location of the elastic axis of the fixed portion and in the mass properties of this portion. The external geometry of both series was identical. The difference between the models in a particular series was in the rotational stiffness of the tip control surface. This stiffness was controlled in a manner similar to that described for series 1. One model of series 3 was equipped with mass balance. This balance was a weighted leading edge which increased the basic weight of the movable surface by about 21 percent. The addition of the mass balance produced a forward shift of the control-surface center of gravity of about 5.4 percent of the mean aerodynamic chord. The method of mounting these models was similar to that for series 1. A photograph of a typical model of this series mounted in the test section is shown as figure 2(b).

L 1 2 6 1

The models of series 4 consisted of seven pairs of matched all-movable control surfaces having a thickness-chord ratio of 5 percent, a single panel aspect ratio of 1.04, and a leading-edge sweep of 46°. All but two of these pairs were equipped with a boom-mounted mass balance located at the 59.3-percent-exposed-semispan station. The added weight of the boom was about 14.5 percent of the basic surface weight. The addition of the balance boom produced a forward shift of the surface center of gravity of about 7.4 percent of the mean aerodynamic chord. These models were sting mounted with the left- and right-hand panels linked through a spring simulating the stiffness of a common actuator system. A photograph of a typical model of this series mounted in the tunnel test section is shown as figure 2(c).

Construction.- A conventional spar and skin type of construction was used for all models. The aluminum skins of the models were stabilized with a core of 0.25- by 0.001-inch hexagonal aluminum honeycomb. The skin thicknesses ranged from 0.004 to 0.012 inch. The basic bending stiffness of the models was determined by the stiffness of the aluminum spar, and the basic torsional stiffness was determined by the thickness of the skin. The rotational stiffness of the movable surfaces was controlled by the use of springs. Certain portions of the honeycomb core were filled with lead to obtain the desired mass properties. The mass-balance booms were constructed of lead-filled 0.010-inch aluminum tubing with a 0.355-inch outside diameter.

Physical properties.- The mass properties of the models tested are given in table I. For the models of the first three series, where the rotational stiffness of the movable portion of the surface was varied by the use of springs and the spring weights varied according to their respective stiffnesses, an average value of the spring weights was used and was included in the weight for each model. Since the actuator system for the models of series 4 was mounted externally, the weight of the actuator system is not included in the weights of the models of this series. Presented in table II is a spanwise breakdown of the mass properties for a typical model of each series.

Prior to the tunnel tests the first three uncoupled mode shapes (bending, torsion, and control rotation) were measured for a typical model of series 1 and 2. The rotational mode was simply a rigid-body rotation of the tip control surface about the hinge line. For the bending and torsion measurements, rotation of the movable surface was prevented by clamping the tip control surface to the inboard portion of

[redacted]

the model. When the rotational mode shape was determined, bending and torsion were prevented by the use of an appropriate clamping system. The measured bending and torsional mode shapes are presented in table III. Although no mode shapes were measured for a sample model of series 3, it is believed that the mode shapes of these models are quite similar to those of the series 2 models. Prior to each tunnel test the first three uncoupled natural frequencies and their corresponding structural damping coefficients were measured for each model tested. These values are tabulated in table IV.

Test Procedure

L1261

The same general procedure was used for all the tests. The determination of a typical flutter point proceeded as follows: With the tunnel evacuated to a low stagnation pressure (1.5 lb/sq in. abs) supersonic flow was established in the test section with the nozzle block set on its optimum setting. The nozzle block was then set for the desired test-section Mach number. The tunnel stagnation pressure was then gradually increased until flutter occurred. At this point the stagnation pressure was held constant and the tunnel conditions necessary to describe the point were recorded. The tunnel stagnation pressure was then rapidly decreased until the flutter stopped. Again, a reading of the tunnel instrumentation was made. The second data point was the one used to describe the flutter condition. Due to tunnel turbulence only a slight penetration was made into the flutter region, and the two sets of data were in close agreement. After the flutter point had been taken the stagnation pressure was decreased to some low value after which the nozzle block was set for a new Mach number and the above procedure repeated at enough points to describe the flutter boundary within the operational characteristics of the tunnel or until the model was destroyed. When no flutter was obtained at a particular Mach number, a data point was taken at the maximum conditions obtainable at the time.

The start and stop of flutter was determined by observing an oscilloscope on which the model bending and pitching strain-gage signals were displayed on the horizontal and vertical axes, respectively. At flutter a Lissajous figure appeared on the oscilloscope. The strain-gage signals were also recorded on a recording oscilloscope and a tape recorder. Visual records of the flutter obtained were made with high-speed motion-picture cameras.

[redacted]

RESULTS AND DISCUSSION

Experimental Results

The basic data obtained are presented in table V and figure 3. The curves shown in figure 3 represent stability boundaries in terms of the variation with Mach number of the dynamic pressure at the flutter condition. The unstable region is above the curve. Since the models in any one series had essentially the same physical properties except in regard to frequency ratio, subsequent comparisons will be made by using the ratio of uncoupled bending frequency to uncoupled rotational frequency (hereafter referred to as frequency ratio) as the important variable between models. Models whose frequency ratios differ by only a small percentage will be assumed to have the same properties.

<u>Series 1</u>.- As shown in figure 3(a) flutter was obtained throughout the tunnel operating range for models with a frequency ratio of about 0.96 and 0.72. Two points were obtained for models with a frequency ratio of 0.59. Also, considerable flutter data were determined for the mass-balanced configuration with a frequency ratio of 0.93. No flutter points were found for models with frequency ratios of 0.53 and 0.45, or for a boom-mounted mass-balanced model with a frequency ratio of 0.74. As indicated by the figure decreasing the frequency ratio has a stabilizing effect in the range below a frequency ratio of 1. For example, a reduction in frequency ratio from about 0.96 to 0.70 approximately triples the dynamic pressure required to produce flutter throughout the test Mach number range. The experimental results indicate an almost linear increase in flutter dynamic pressure with Mach number.

The test results indicate a stabilizing effect of mass balance on the flutter characteristics. This is best illustrated by comparing the flutter data for an unbalanced model with a frequency ratio of about 0.70 with the no-flutter data for the balanced model with a frequency ratio of 0.74. Comparing the data for the unbalanced model with a frequency ratio of about 0.96 with that of the balanced model with a frequency ratio of 0.93 indicates that mass balance becomes more effective in stabilizing the model with increasing Mach number. However, the effect of mass balance has probably been magnified to some extent because the addition of the balance boom resulted in a slightly lower frequency ratio, which has also been shown to have a stabilizing effect. The beneficial effect of mass balance becomes more pronounced with decreasing values of frequency ratio.

The type of flutter mode found for the models of this series was primarily a combination of bending and control rotation. At the largest frequency ratio tested the rotation predominated. With decreasing frequency ratio the proportion of bending contained in the mode became larger.

[redacted]

Series 2.- Reference to figure 3(b) shows that only a limited number of flutter points were determined for the models of this series. It should be noted that the flutter point at $M = 1.57$ for the model with a frequency ratio of 0.57 is questionable since the model experienced some severe aerodynamic loading at the tunnel start, possibly weakening the model structurally. Consequently, the flutter point at this Mach number for the model with a frequency ratio of 0.58 is believed to be more representative of the flutter condition for models having this ratio. As shown in the figure the effect of decreasing frequency ratio has a stabilizing effect over the range of Mach numbers investigated. Also, there appears to be a more rapid increase of flutter dynamic pressure with Mach number than was found for the models of series 1. The flutter mode for these models was essentially a combination of bending and control rotation.

Series 3.- The flutter stability boundaries for the models of this series are presented in figure 3(c). The variation of flutter dynamic pressure with Mach number is far more pronounced for the models of series 3 than that found for the models of series 1. In fact, the flutter dynamic pressure for the model with frequency ratio of 0.60 appears to be approaching an asymptote around $M = 2.1$. An examination of some of the steady-state aerodynamic characteristics, particular emphasis being placed on the variation of the tip-control hinge-moment coefficient with Mach number, of series 1 and of series 2 and 3 was made in an effort to explain the different variation of flutter dynamic pressure with Mach number found for the two planforms. This examination gave no indication that dissimilar flutter characteristics should be expected. The models of this series also exhibit the stabilizing effect of reducing the frequency ratio. The data for the mass-balanced configuration appear to indicate a stabilizing effect since it would be expected that an unbalanced model with a frequency ratio of 0.77 would flutter at a lower dynamic pressure than a model with a frequency ratio of 0.60, and no flutter points were obtained for the balanced model at dynamic pressures about 1.8 times those for the unbalanced model with a frequency ratio of 0.60.

Series 4.- Only two flutter points were determined for the models tested of this series. Both of these points were determined for models which were not equipped with mass-balance booms and had a frequency ratio of about 1.73. For the flutter point at $M = 1.90$ the model began to flutter in a limited-amplitude antisymmetrical bending-rotational mode. This beginning of flutter was unnoticed since the strain-gage signals which were being monitored on the oscilloscope were insensitive to antisymmetrical modes. Consequently, the tunnel pressure was allowed to continue to increase. After a small increase in pressure the flutter mode changed to a diverging symmetrical mode resulting in the destruction of the model. The model which was fluttered at $M = 2.2$ was

[redacted]

damaged at the beginning of flutter. The nature of the flutter mode for this model was not determined.

Calculated Results

Theoretical flutter calculations were made for all of the models of series 1 and for some of the models of series 2 and 3. These calculations were made by using piston-theory aerodynamics with the effects of thickness included (ref. 2) and two uncoupled modes (bending and control-surface rotation) with zero structural damping.

L
1
2
5
1

The results of flutter calculations for the models of series 1 are presented in figures 4 and 5. As shown in figure 4 where the variation of the calculated flutter velocity index parameter $\frac{V}{b\omega_\theta\sqrt{\mu}}$ with Mach number is compared with the corresponding experimental data, good agreement was found between theory and experiment. The theoretical results for the unbalanced surfaces become more unconservative with decreasing frequency ratio. Conservative results were found for the model equipped with the mass-balance boom. The calculated flutter frequencies are also in good agreement with experiment. This can be seen in figure 5 where the variation with Mach number of the ratio of measured to calculated flutter frequency is presented.

The results of calculations for the models of series 2 and 3 were highly unconservative. This unconservatism is illustrated in figure 6 where a comparison of measured and calculated variations with Mach number of the velocity index parameter are presented for the model of series 3 with a frequency ratio of 0.60. It has been pointed out that the variation of the experimental flutter dynamic pressure with Mach number was quite different for the models of series 1 and of series 2 and 3. The analysis used predicted a different flutter behavior for the two planforms; however, this analysis gave good results for series 1 and unconservative results for series 2 and 3. The calculated flutter frequency was about 20 percent higher than that found experimentally.

CONCLUDING REMARKS

Wind-tunnel tests have been completed on four series of low-aspect-ratio surfaces in the Mach number range from 1.49 to 2.87. Three of the series tested consisted of a cantilevered inboard panel with a tip control surface forming the outboard portion of the configuration. The fourth series consisted of sting-mounted matched pairs of all-movable control surfaces linked through a spring simulating the stiffness of a common actuator system. Models of each series with several different values of the ratio of uncoupled bending frequency to uncoupled rotational frequency were tested. Some of the models tested were equipped with mass balance. Within the range covered, it was found that the lowest flutter dynamic pressures were obtained when the ratio of uncoupled bending frequency to uncoupled rotational frequency was near 1 and that flutter may be eliminated or the dynamic pressure at flutter may be increased by the use of mass balance, the effect being greater at the lower frequency ratios.

Calculations based on piston theory gave good results for all of L
the models of one of the series with the movable surface forming the 1
outboard portion. Similar calculations for the other two series with 2
the tip control surface were highly unconservative. The reason for 6
this unconservatism was not determined. 1

Langley Research Center,
National Aeronautics and Space Administration,
Langley Field, Va., June 14, 1961.

REFERENCES

1. Morgan, Homer G., Figge, Irving E., and Presnell, John G., Jr.: Investigation of Flutter Characteristics of Three Low-Aspect-Ratio All-Movable Half-Span Control Surfaces at Mach Numbers From 1.49 to 2.87. NACA RM L58B20, 1958.

2. Ashley, Holt, and Zartarian, Garabed: Piston Theory - A New Aerodynamic Tool for the Aeroelastician. Jour. Aero. Sci., vol. 23, no. 12, Dec. 1956, pp. 1109-1118.

TABLE I.- MODEL MASS DATA

(a) Series 1

Model	Portion of model	Mass-balance configuration	Weight, lb	Pitch inertia about center of gravity, lb-in.^{2}	Pitch inertia about hinge line, lb-in.^{2}	Center of gravity x, in.	Center of gravity y, in.
1a	Fixed Movable Total	None	2.794 .440 3.234	194.8 5.37 206.7	5.96	13.82 6.945 13.25	6.436 16.496 7.806
1b and 1h	Fixed Movable Total	None	2.805 .463 3.268	145.8 5.98 158.1	6.66	13.60 6.885 13.03	6.726 16.506 8.116
1c and 1g	Fixed Movable Total	None	2.885 .436 3.321	161.0 5.71 172.2	6.34	13.44 6.975 12.94	6.186 16.516 7.546
1d and 1e	Fixed Movable Total	None	2.805 .440 3.245	145.8 5.44 157.2	6.02	13.60 6.865 13.06	6.726 16.556 8.056
1f	Fixed Movable Total	None	3.030 .463 3.493	141.0 5.98 152.7	6.66	13.40 6.885 12.90	6.286 16.506 7.646
1i	Fixed Movable Total	Boom mounted	3.030 .529 3.559	141.0 8.09 153.1	8.17	13.40 7.375 12.96	6.286 16.506 7.856
1j	Fixed Movable Total	Boom mounted	3.049 .527 3.576	183.8 7.40 195.0	7.48	13.32 7.385 12.89	6.286 16.816 7.786

TABLE I.- MODEL MASS DATA - Continued

(b) Series 2

Model	Portion of model	Mass-balance configuration	Weight, lb	Pitch inertia about center of gravity, lb-in.^{2}	Pitch inertia about hinge line, lb-in.^{2}	Center of gravity	
						x, in.	y, in.
2a	Fixed Movable Total	None	0.793 .223 1.016	12.56 2.11 14.67	2.25	7.98 6.80 7.99	4.295 10.745 5.735
2b	Fixed Movable Total	None	0.788 .223 1.011	11.84 1.98 13.85	2.20	8.19 6.57 8.118	4.385 10.755 5.558
2c	Fixed Movable Total	None	0.806 .223 1.029	10.97 1.76 12.86	1.96	8.70 6.66 8.52	4.385 10.725 5.775
2d	Fixed Movable Total	None	0.788 .223 1.011	9.32 1.98 11.52	2.20	8.92 6.57 8.67	4.505 10.755 5.865
2e	Fixed Movable Total	None	0.774 .222 .996	10.23 2.08 13.32	2.28	8.11 6.85 8.05	4.435 10.625 5.815

L1261

TABLE I.- MODEL MASS DATA - Continued

(c) Series 3

Model	Portion of model	Mass-balance configuration	Weight, lb	Pitch inertia about center of gravity, lb-in.^{2}	Pitch inertia about hinge line, lb-in.^{2}	Center of gravity	
						x, in.	y, in.
3a, 3b, and 3c	Fixed	None	1.084	14.03	2.07	8.38	2.585
	Movable		.223	1.38		7.80	10.645
	Total		1.307	15.96		8.30	3.975
3d	Fixed	Heavy leading edge	1.131	12.67	2.89	8.44	2.605
	Movable		.272	2.89		8.78	10.105
	Total		1.403	15.60		8.52	4.055

[redacted]

TABLE I.- MODEL MASS DATA - Concluded

(d) Series 4

Model	Portion of model	Mass-balance configuration	Weight, lb	Pitch inertia about center of gravity, lb-in.^{2}	Pitch inertia about hinge line, lb-in.^{2}	Center of gravity	
						x, in.	y, in.
4a	Left hand Right hand	None None	0.380 .380	5.11 5.15	5.22 5.28	8.24 8.18	2.65 2.64
4b	Left hand Right hand	None None	0.382 .313	5.04 4.99	5.19 5.05	8.16 8.35	2.70 2.75
4c	Left hand Right hand	Boom mounted Boom mounted	0.449 .447	6.28 6.46	6.29 6.46	8.96 8.92	3.03 3.10
4d	Left hand Right hand	Boom mounted Boom mounted	0.417 .398	6.79 6.66	6.79 6.66	8.74 8.78	3.53 3.55
4e	Left hand Right hand	Boom mounted Boom mounted	0.444 .425	7.86 7.62	7.89 7.64	8.52 8.57	3.63 3.63
4f	Left hand Right hand	Boom mounted Boom mounted	0.444 .444	6.56 6.86	6.57 6.87	8.75 8.82	3.06 3.10
4g	Left hand Right hand	Boom mounted Boom mounted	0.385 .398	6.79 6.60	6.80 6.61	8.92 8.92	3.47 3.54

L1261

[redacted]

L1251

TABLE II.- TYPICAL SPANWISE DISTRIBUTION OF MASS, MOMENT OF INERTIA, AND CENTER-OF-GRAVITY LOCATION

(a) Series 1 without mass balance

Span interval, fraction of span	m, slugs	I_α, slug-ft^2	x, ft	y, ft
0 to 0.0995	0.02453	0.01736	1.5350	0.0752
.0995 to .195	.007919	.005129	1.2550	.2970
.195 to .290	.006429	.003623	1.1892	.4880
.290 to .386	.005845	.002704	1.1000	.6788
.386 to .466	.005624	.001803	1.0108	.8647
.466 to .577	.03039	.001620	.8950	1.0567
[a].577 to .581				
.581 to .689	.007484	.0009446	.8208	1.2347
.689 to .797	.004177	.0002480	.6048	1.4813
.797 to .905	.001522	.00005823	.2981	1.6672
.905 to 1.0	.000357	.00004313	.1315	1.8587

[a]0.10-inch gap between fixed and all-movable surfaces.

 [redacted]

TABLE II.- TYPICAL SPANWISE DISTRIBUTION OF MASS, MOMENT OF INERTIA, AND CENTER-OF-GRAVITY LOCATION - Continued

(b) Series 2 without mass balance

L 1 2 6 1

Span interval, fraction of span	m, slugs	I_α, slug-ft^2	x, ft	y, ft
0 to 0.0673	0.007143	0.0009985	0.6308	0.02375
.0673 to .134	.001646	.0002825	.7883	.1271
.134 to .201	.001366	.0002502	.7625	.2187
.201 to .268	.004441	.0002221	.7333	.2979
.268 to .336	.001553	.0001898	.7117	.4004
.336 to .403	.001739	.0001682	.6950	.4971
.403 to .471	.002143	.0001467	.6858	.5804
.471 to .538	.007547	.0002372	.6758	.6812
[a].538 to .541				
.541 to .636	.003680	.0002459	.6397	.7604
.636 to .731	.001304	.0001100	.5000	.8962
.731 to .826	.0007671	.00003990	.3683	1.0279
.826 to .921	.001025	.00001510	.3206	1.1604
.921 to 1.0	.0001180	.00000043	.1948	1.2462

[a]0.062-inch gap between fixed and all-movable surfaces.

[redacted]

TABLE II.- TYPICAL SPANWISE DISTRIBUTION OF MASS, MOMENT

OF INERTIA, AND CENTER-OF-GRAVITY LOCATION - Concluded

(c) Series 3 without mass balance

Span interval, fraction of span	m, slugs	I_α, slug-ft^2	x, ft	y, ft
0 to 0.134	0.01876	0.001911	0.7233	0.08125
.134 to .268	.004668	.0004702	.6667	.2729
.268 to .403	.003043	.0003257	.6992	.4446
.403 to .538	.007202	.0002847	.6533	.6704
[a].538 to .541				
.541 to .636	.003680	.0002459	.6397	.7604
.636 to .731	.001304	.0001100	.5000	.8962
.731 to .826	.0007671	.00003990	.3683	1.0279
.826 to .921	.001025	.00001510	.3206	1.1604
.921 to 1.0	.0001180	.00000043	.1948	1.2462

[a]0.062-inch gap between fixed and all-movable surfaces.

(d) Series 4 with mass balance

Span interval, fraction of span	m, slugs	I_α, slug-ft^2	x, ft	y, ft
0 to 0.250	0.006957	0.0005737	0.7458	0.0750
.250 to .500	.003944	.0003580	.6950	.3483
.500 to .750	.005000	.0003709	.6665	.5450
.750 to 1.0	.0006211	.000005607	.1655	.7542

[redacted]

[redacted]

TABLE III.- UNCOUPLED NATURAL MODE SHAPES FOR TYPICAL

MODELS OF SERIES 1 AND 2

(a) Series 1, bending

$\left[\omega_h = 468.1;\ g_h = 0.015\right]$

Fraction span	Fraction chord				
	0.10	0.30	0.50	0.70	0.90
0.899	1.000	1.096	-----	-----	-----
.865	.939	1.009	-----	-----	-----
.781	.772	.789	1.000	0.877	-----
.697	.614	.614	.754	.719	0.895
.614	.482	.456	.570	.579	.702
.530	.351	.342	.404	.456	.535
.446	.237	.237	.281	.351	.386
.362	.140	.158	.175	.228	.263
.279	.070	.088	.096	.149	.175
.195	.026	.044	.044	.088	.105
.111	-----	-----	.018	.044	.070

I
1
2
6
1

(b) Series 1, torsion

$\left[\omega_\alpha = 1{,}011.6;\ g_\alpha = 0.012\right]$

Fraction span	Fraction chord				
	0.10	0.30	0.50	0.70	0.90
0.899	1.000	-13.332	-------	-------	-------
.865	5.666	-8.333	-------	-------	-------
.781	17.665	2.000	-13.332	-31.330	-------
.697	28.331	10.999	-4:666	-24.998	-49.328
.614	36.663	17.665	.333	-19.665	-42.329
.530	38.330	21.665	5.000	-14.999	-36.663
.446	36.330	23.331	7.999	-10.666	-31.664
.362	32.997	22.998	10.000	-6.999	-27.331
.279	27.664	20.998	10.332	-4.666	-23.998
.195	20.331	18.332	10.000	-3.000	-20.998
.111	11.666	14.665	8.999	-1.667	-18.332

[redacted]

TABLE III.- UNCOUPLED NATURAL MODE SHAPES FOR TYPICAL

MODELS OF SERIES 1 AND 2 - Concluded

(c) Series 2, bending

$\left[\omega_h = 659.7;\ g_h = 0.023\right]$

Fraction span	Fraction chord		
	0.10	0.50	0.90
0.903	1.000	-----	-----
.798	.801	0.765	-----
.672	.686	.556	0.693
.609	.490	.461	.588
.545	.405	.379	.490
.507	.353	.333	.438
.419	.252	.242	.327
.292	.147	.131	.196
.166	.062	.049	.092
.040	.013	.007	.033

(d) Series 2, torsion

$\left[\omega_\alpha = 1{,}470.3;\ g_\alpha = 0.028\right]$

Fraction span	Fraction chord		
	0.10	0.50	0.90
0.903	1.000	------	------
.798	1.010	-0.164	------
.672	1.060	-.193	------
.609	1.100	-.214	------
.545	.836	-.179	-1.614
.507	.750	-.150	-1.286
.419	.607	-.100	-1.050
.292	.429	-.043	-.729
.166	.250	-.014	-.414
.040	.086	------	-.157

[redacted]

[redacted]

TABLE IV.- MODEL FREQUENCY DATA

(a) Series 1

Model	ω_h/ω_θ	ω_h	g_h	ω_θ	g_θ	ω_α	g_α
1a	0.45	436	0.020	979	-----	1,051	0.038
1b	.53	494	.009	926	-----	1,014	.027
1c	.59	464	.034	791	0.033	1,018	.044
1d	.70	494	.009	708	.042	1,014	.027
1e	.71	494	.009	699	.027	1,014	.027
1f	.74	495	.016	664	.025	1,000	.094
1g	.94	489	.018	518	.033	1,060	.018
1h	.98	497	.015	505	.032	1,028	.015
1i	.74	446	.033	599	.023	937	.040
1j	.93	455	.027	488	.025	955	.010

L
1
2
6
1

(b) Series 2

Model	ω_h/ω_θ	ω_h	g_h	ω_θ	g_θ	ω_α	g_α
2a	0.52	628	0.025	1,219	0.120	1,508	0.061
2b	.57	677	.040	1,191	.064	1,374	.045
2c	.58	704	.016	1,219	.120	1,558	.060
2d	.73	729	.020	1,005	.080	1,389	.041
2e	.81	716	.018	886	.110	1,483	.067

[redacted]

L
1
2
6
1

TABLE IV.- MODEL FREQUENCY DATA - Concluded

(c) Series 3

Model	ω_h/ω_θ	ω_h	g_h	ω_θ	g_θ	ω_α	g_α
3a	0.50	605	0.018	1,219	0.120	1,420	0.052
3b	.60	605	.018	1,005	.080	1,420	.052
3c	.64	605	.018	943	.080	1,420	.052
3d	.77	616	.017	804	.068	1,571	.058

(d) Series 4

Model	ω_h/ω_θ	ω_h	g_h	ω_θ	g_θ	ω_β	g_β
4a	1.72	1,339	0.080	780	0.098	1,167	0.120
4b	1.74	1,399	.057	806	.130	1,297	.089
4c	.83	842	-----	1,010	-----	-----	-----
4d	.84	842	-----	1,005	-----	-----	-----
4e	1.50	1,024	.024	682	.121	1,068	.071
4f	2.08	1,047	.070	503	.136	1,100	.050
4g	2.12	1,051	.033	495	.080	1,026	.057

[redacted]

TABLE V.- BASIC TEST DATA

(a) Series 1

Model	ω_h/ω_θ	M	q, lb/sq ft	V, ft/sec	ρ, slugs/cu ft	ω_f, radians/sec	ω_f/ω_θ	μ	$\frac{V}{b\omega_\theta\sqrt{\mu}}$	Remarks
1a	0.45	1.57	2,134	1,524	18.40×10^{-4}			8.96	0.586	No flutter
		1.90	2,172	1,717	14.70			11.21	.590	No flutter
		2.23	2,361	1,872	13.48			12.23	.616	No flutter
1b	0.53	2.40	1,567	1,989	7.92×10^{-4}			21.05	0.527	No flutter
		2.60	1,640	2,061	7.72			21.60	.540	No flutter
		2.87	1,563	2,144	6.79			24.56	.526	No flutter
1c	0.59	1.90	2,023	1,717	13.73×10^{-4}	613	0.775	12.33	0.698	
		2.20	2,165	1.860	12.53	636	.804	13.52	.721	
		2.40	1,567	1,981	7.99			21.20	.613	No flutter
1d	0.70	2.40	1,133	1,974	5.82×10^{-4}	561	0.792	28.41	0.589	
1e	0.71	1.57	947	1,521	8.18×10^{-4}	583	0.835	20.22	0.546	
		1.90	1,000	1,714	6.81	593	.849	24.30	.560	
1f	0.74	2.60	1,104	2,061	5.20×10^{-4}	576	0.867	34.23	0.598	
		2.87	1,105	2,144	4.81	566	.852	37.05	.598	
1g	0.94	2.40	310	1,981	1.58×10^{-4}	530	1.024	106.75	0.417	
		2.60	339	2,053	1.61	530	1.024	105.20	.436	
		2.87	331	2,136	1.45	533	1.029	116.75	.432	
1h	0.98	1.57	282	1,497	2.52×10^{-4}	535	1.060	66.15	0.410	
		1.90	3,302	1,702	2.08	535	1.060	80.15	.423	
1i	0.74	1.57	2,147	1,543	18.04×10^{-4}			10.06	0.916	No flutter
		2.20	2,104	1,883	11.88			15.28	.906	No flutter
1j	0.93	1.57	321	1,543	2.70×10^{-4}	473	0.968	67.50	0.434	
		1.63	323	1,581	2.65	473	.968	68.80	.440	
		1.90	381	1,742	2.51	473	.968	72.60	.472	
		1.99	369	1,788	2.31	473	.968	78.90	.465	
		2.20	420	1,886	2.36	473	.968	77.20	.496	
		2.40	497	1,981	2.53	468	.958	72.00	.539	
		2.43	489	1,992	2.46	468	.958	74.10	.534	

[redacted]

[redacted]

L1261

TABLE V.- BASIC TEST DATA - Continued

(b) Series 2

Model	ω_h/ω_θ	M	q, lb/sq ft	V, ft/sec	ρ, slugs/cu ft	ω_f, radians/sec	ω_f/ω_θ	μ	$\frac{V}{b\omega_\theta\sqrt{\mu}}$	Remarks
2a	0.52	1.67	2,404	1,620	18.33×10^{-4}			11.64	0.745	No flutter
		1.87	2,738	1,737	18.16			11.74	.752	No flutter
2b	0.57	1.57	1,843	1,547	15.43×10^{-4}	792	0.664	13.75	0.634	
2c	0.58	1.57	2,062	1,556	17.05×10^{-4}	842	0.691	12.65	0.648	
		2.17	2,882	1,886	16.22			13.30	.767	No flutter
2d	0.73	1.57	706	1,556	5.83×10^{-4}	787	0.782	36.38	0.465	
		1.87	1,181	1,737	7.83	812	.808	27.10	.605	
		2.16	1,209	1,881	6.83	802	.797	31.04	.608	
2e	0.81	1.57	348	1,556	2.88×10^{-4}	749	0.845	72.55	0.373	
		1.87	598	1,737	3.96	779	.879	52.80	.488	

[redacted]

[redacted]

TABLE V.- BASIC TEST DATA - Continued

(c) Series 3

Model	ω_h/ω_θ	M	q, lb/sq ft	V, ft/sec	ρ, slugs/cu ft	ω_f, radians/sec	ω_f/ω_θ	μ	$\frac{V}{b\omega_\theta\sqrt{\mu}}$	Remarks
3a	0.50	1.57	1,299	1,556	10.74×10^{-4}	759	0.623	25.53	0.458	
		1.87	2,624	1,737	17.40	802	.659	15.76	.650	
3b	0.60	1.57	735	1,556	6.08×10^{-4}	724	0.720	45.10	0.417	
		1.87	1,137	1,737	7.54	746	.742	36.38	.518	
		1.97	1,834	1,791	11.45	769	.765	23.96	.660	
		2.07	1,667	1,840	9.86	739	.735	27.81	.628	
		2.16	2,988	1,881	16.90			16.24	.841	No flutter
		2.54	1,648	2,032	7.89			34.38	.624	No flutter
		2.87	1,728	2,135	7.58			36.19	.639	No flutter
3c	0.64	1.57	611	1,556	5.06×10^{-4}	709	0.752	54.20	0.542	
		1.87	949	1,737	6.29	729	.773	43.60	.590	
		2.16	1,522	1,881	8.61			31.87	.639	No flutter
3d	0.77	1.47	1,195	1,488	10.81×10^{-4}			27.22	0.641	No flutter
		1.57	1,229	1,556	10.61			27.75	.664	No flutter

[redacted]

L 1 2 6 1

[redacted]

TABLE V.- BASIC TEST DATA - Concluded

(d) Series 4

Model	ω_h/ω_θ	M	q, lb/sq ft	V, ft/sec	ρ, slugs/cu ft	ω_f, radians/sec	ω_f/ω_θ	μ (a)	$\frac{V}{b\omega_\theta\sqrt{\mu}}$	Remarks
4a	1.72	2.20	1,916	1,883	10.82×10^{-4}	1,269	1.088	15.97	1.383	
4b	1.74	1.57	1,582	1,543	13.31×10^{-4}			11.87	1.280	No flutter
		1.90	1,732	1,739	11.48	880	0.678	13.76	1.340	
		1.90	1,882	1,739	12.47	880	.678	12.67	1.395	
		2.60	1,640	2,053	7.80			20.25	1.304	No flutter
4c	0.83	1.65	2,280	1,610	17.55×10^{-4}			11.61	1.078	No flutter
		2.16	2,580	1,880	15.30			13.31	1.175	No flutter
4d	0.84	2.54	1,574	2,032	7.61×10^{-4}			24.34	0.945	No flutter
		2.76	1,624	2,100	7.35			25.21	.959	No flutter
4e	1.50	1.57	1,586	1,543	13.34×10^{-4}			14.81	1.395	No flutter
		1.90	1,867	1,739	12.37			15.97	1.470	No flutter
		2.20	2,044	1,883	11.55			17.11	1.537	No flutter
4f	2.08	2.20	2,287	1,883	12.92×10^{-4}			15.63	2.182	No flutter
4g	2.12	1.57	1,817	1,543	15.29×10^{-4}			11.64	2.104	No flutter

[a]Includes mass and representative volume of both right- and left-hand panels.

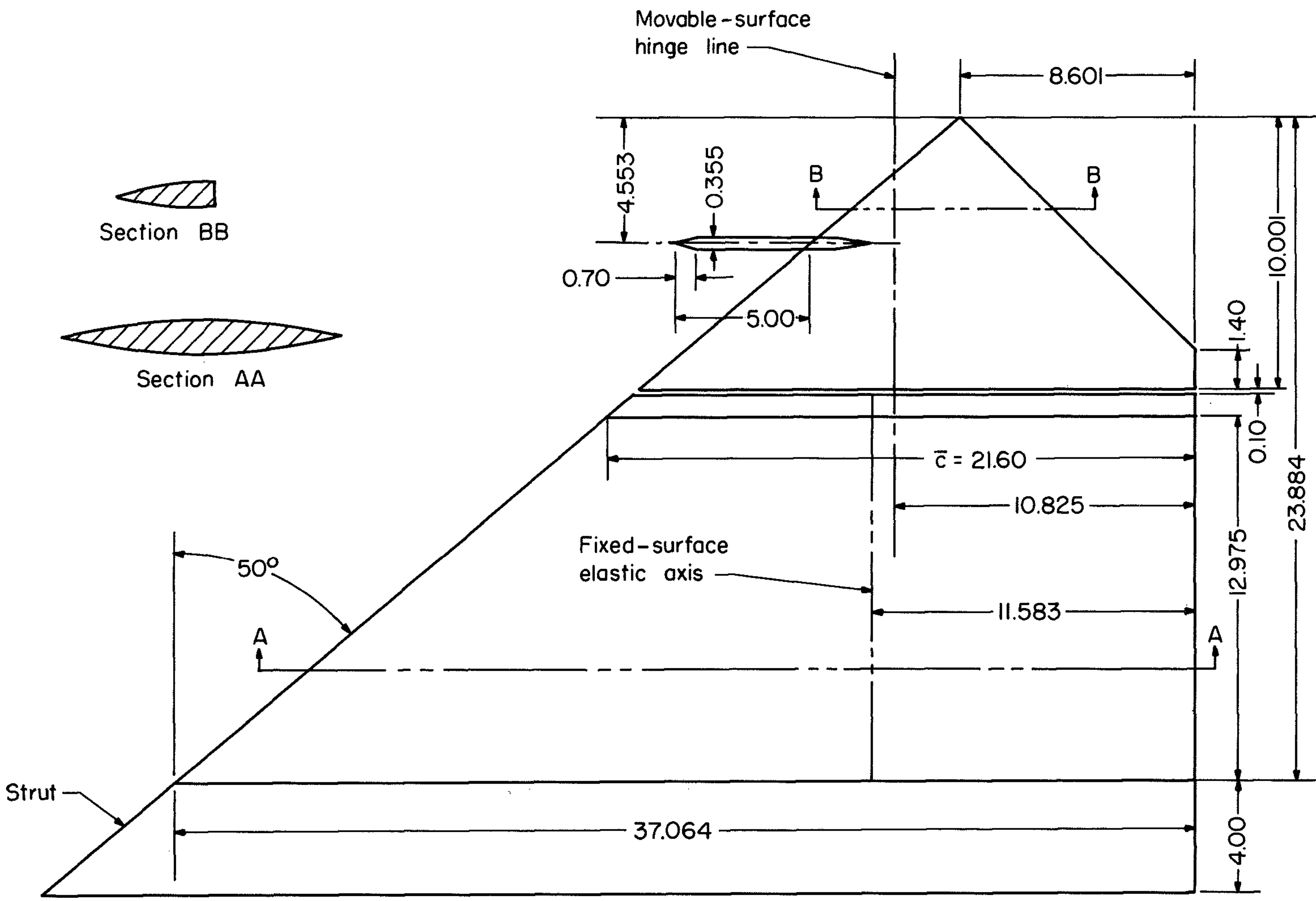

(a) Series 1.

Figure 1.- Drawings of models, showing pertinent linear dimensions in inches.

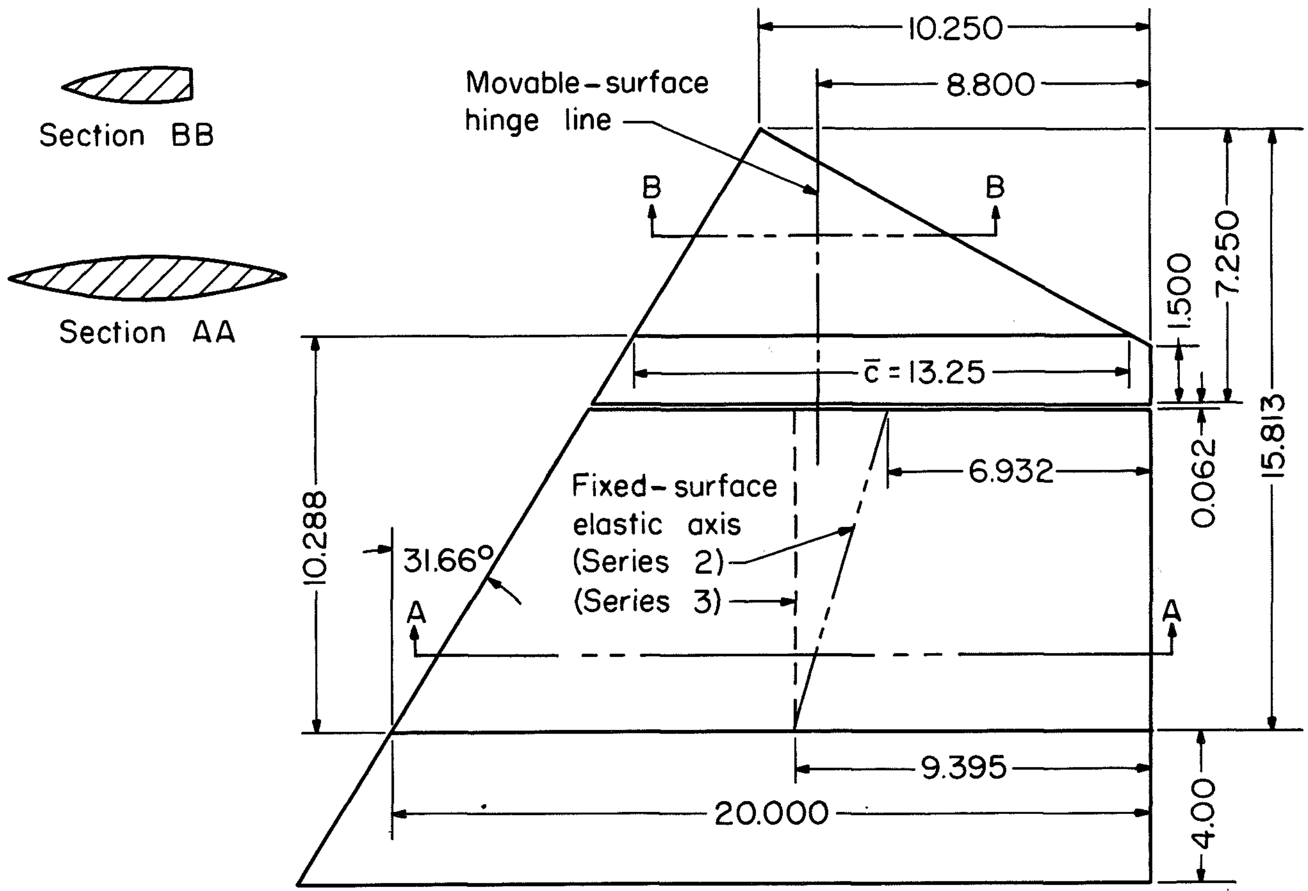

(b) Series 2 and 3.

Figure 1.- Continued.

[redacted]

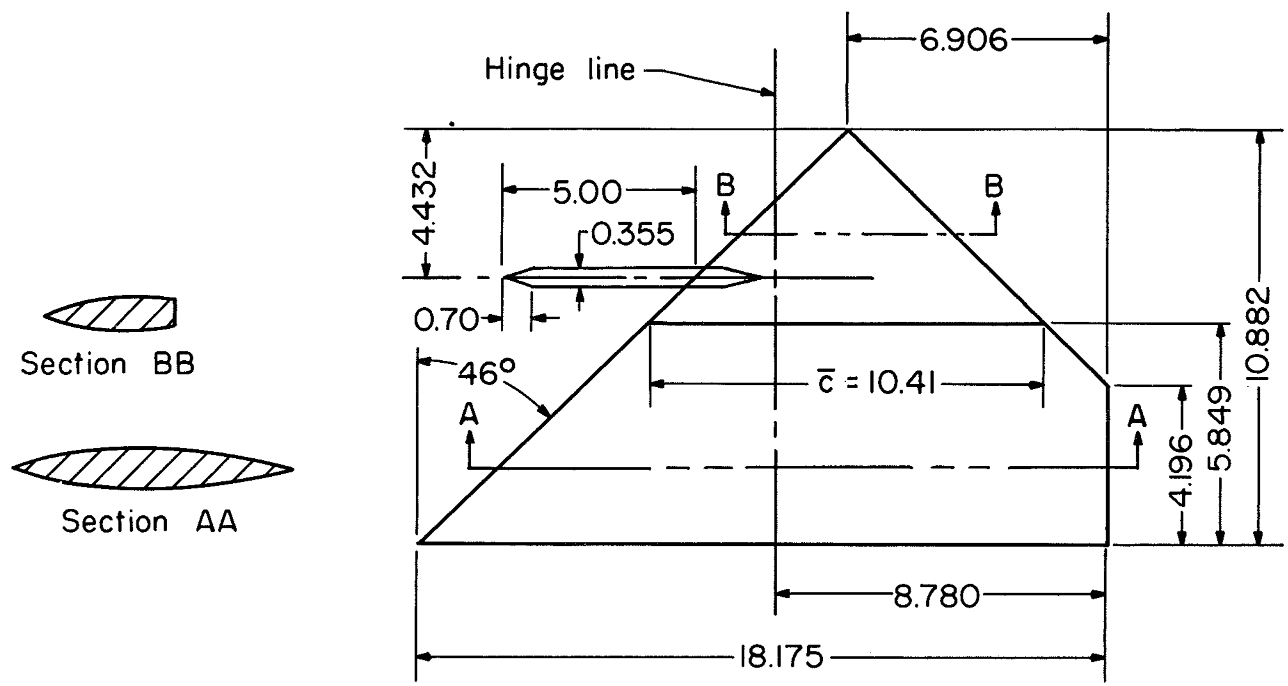

(c) Series 4 (one panel).

Figure 1.- Concluded.

L-1261

[redacted]

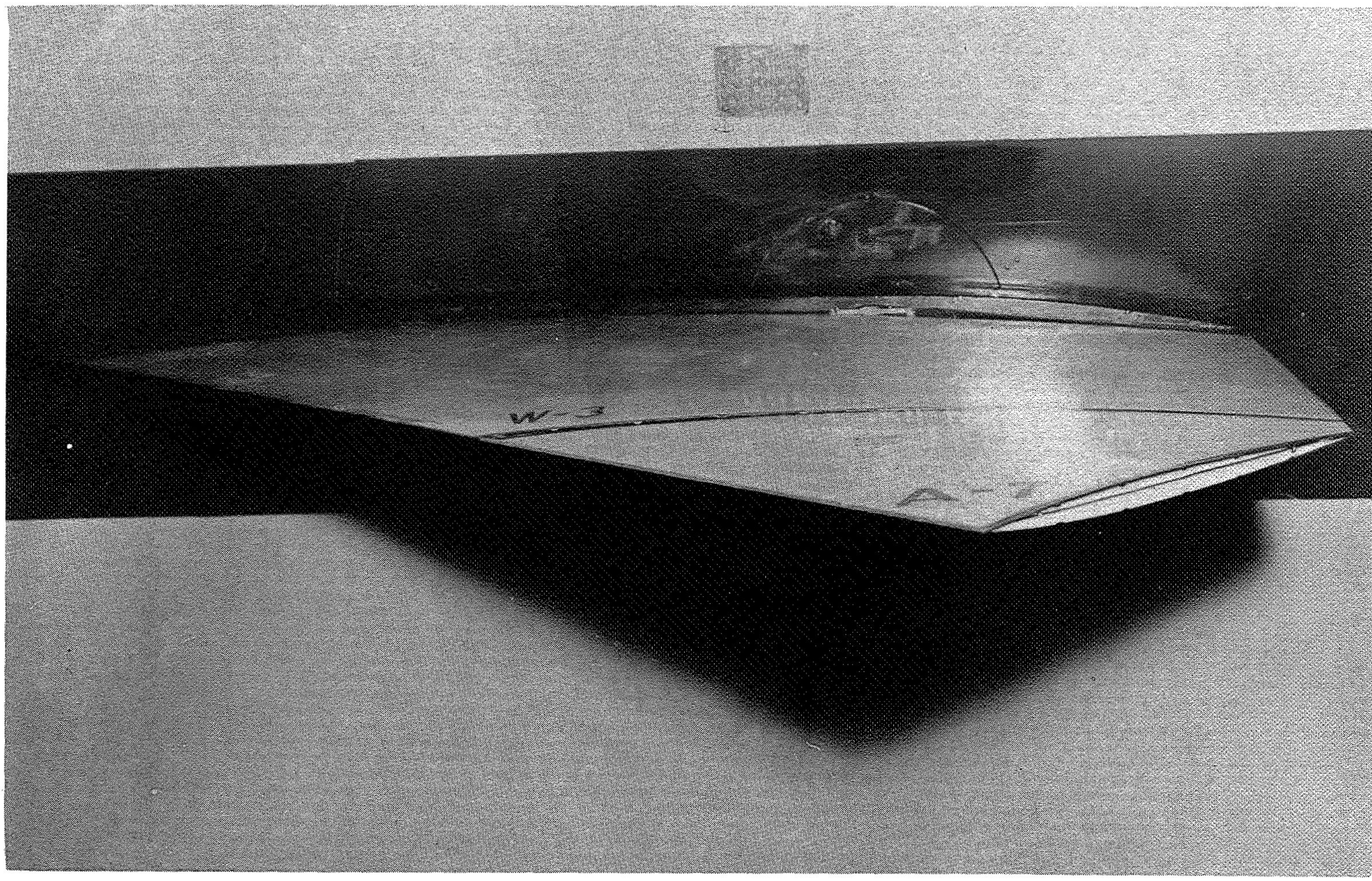

(a) Series 1. L-59-537.1

Figure 2.- Photographs of typical models mounted in wind tunnel.

[redacted]

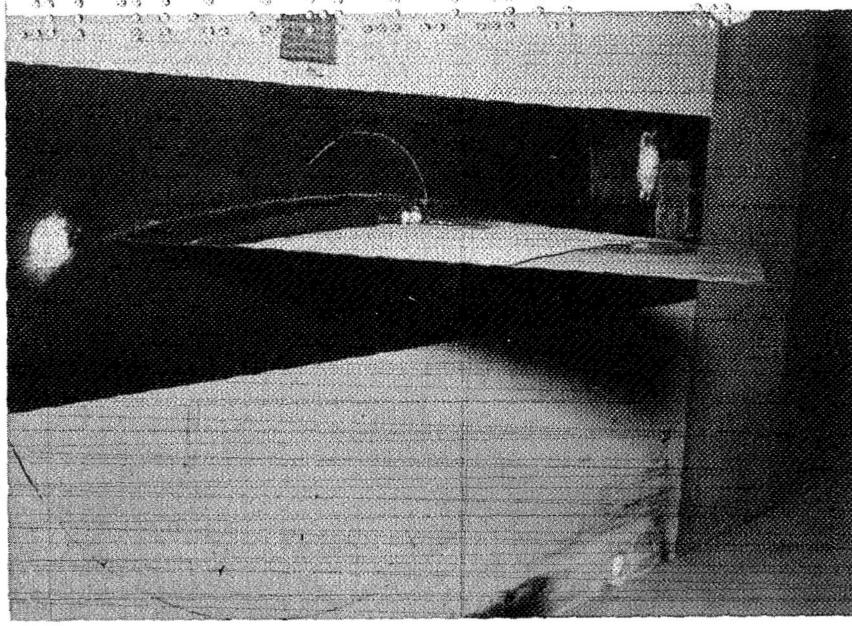

(b) Series 2 and 3.

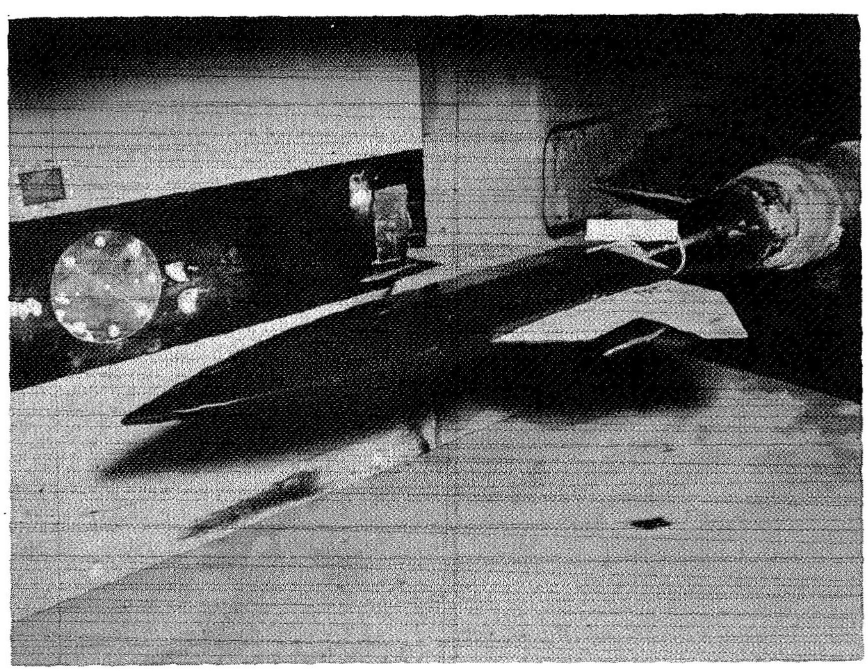

(c) Series 4. L-61-2244

Figure 2.- Concluded.

L-1261

[redacted]

L-1261

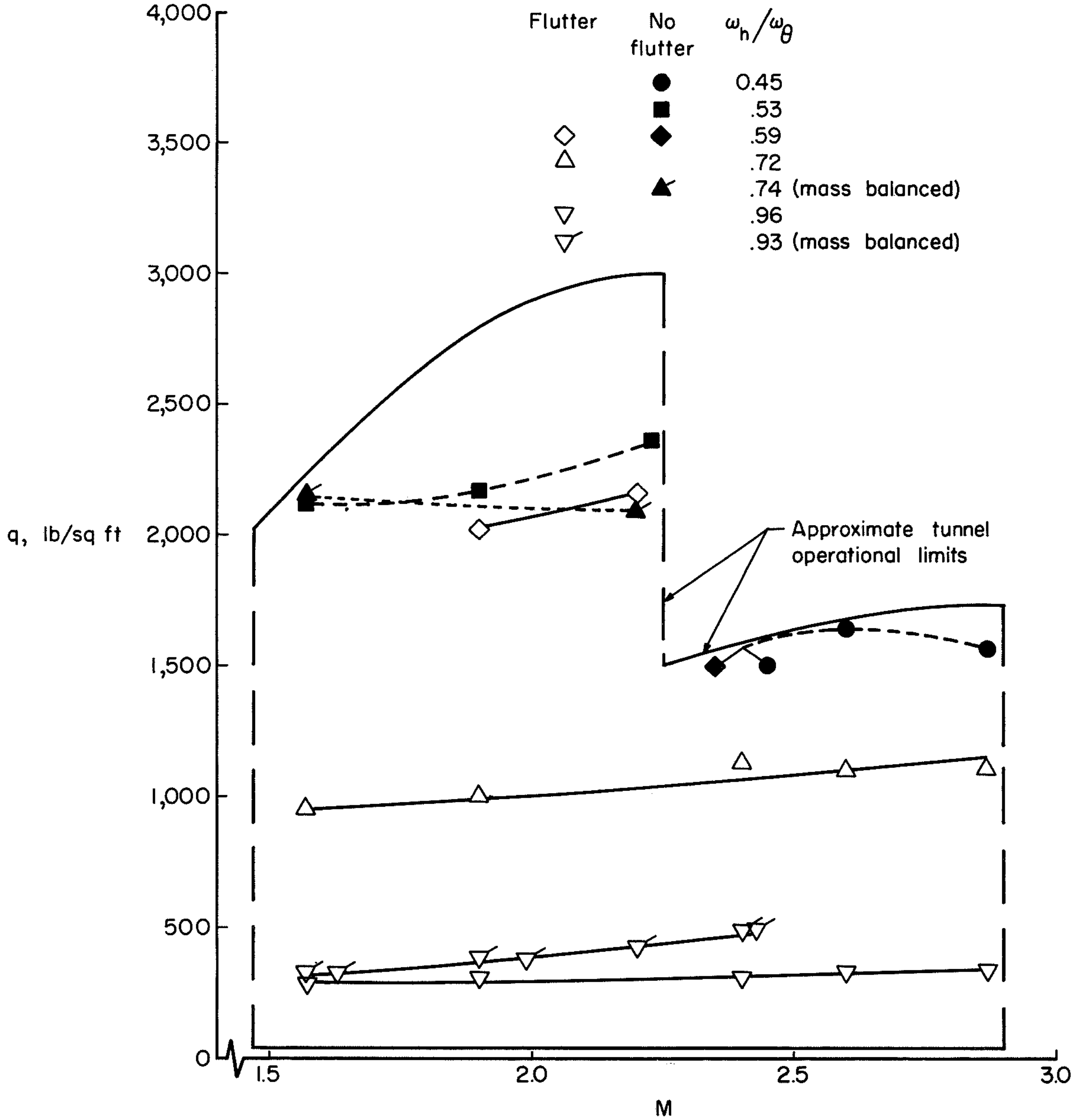

(a) Series 1.

Figure 3.- Variation of experimental dynamic pressure at flutter with Mach number.

[redacted]

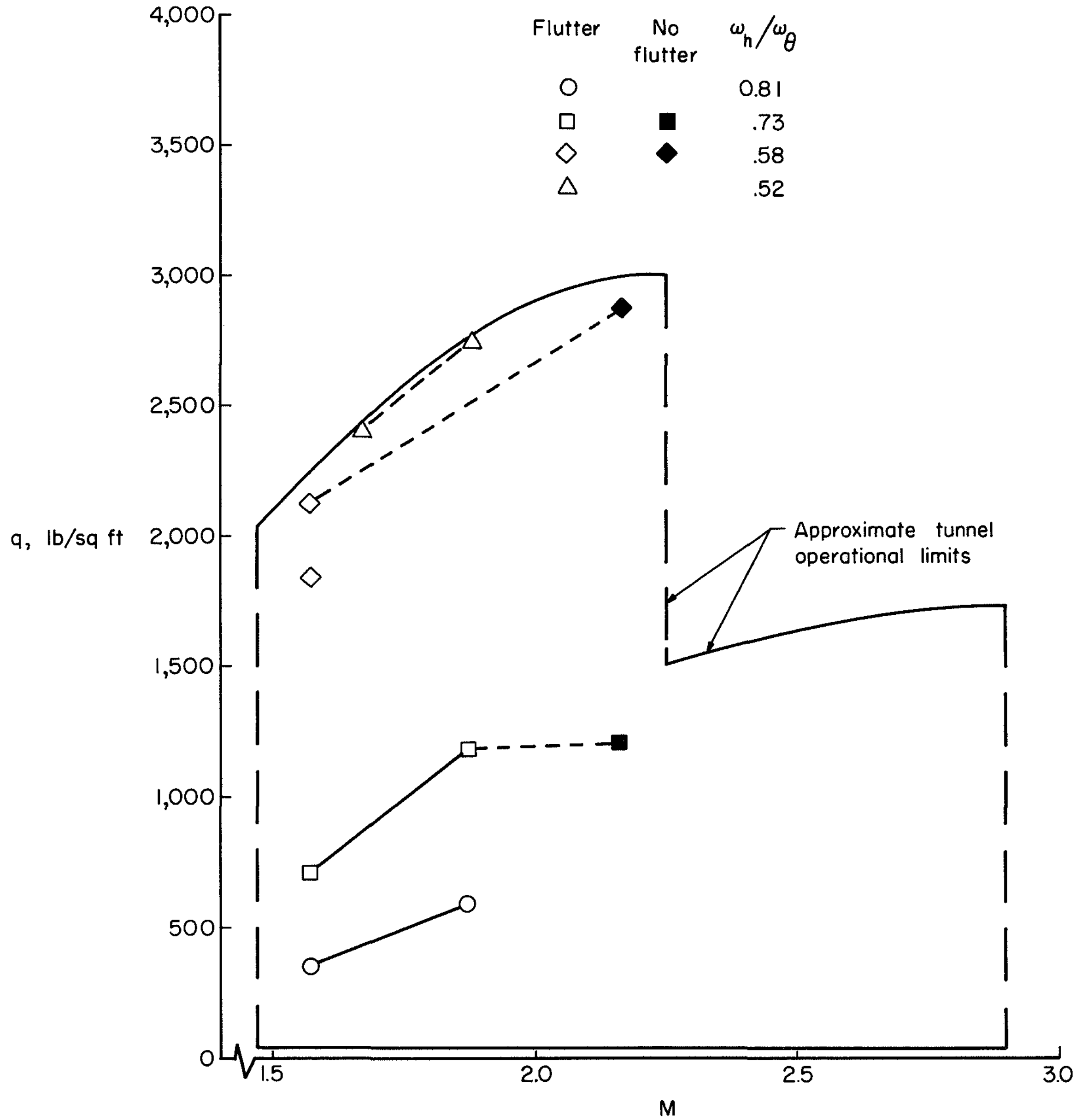

(b) Series 2.

Figure 3.- Continued.

L-1261

[redacted]

L-1261

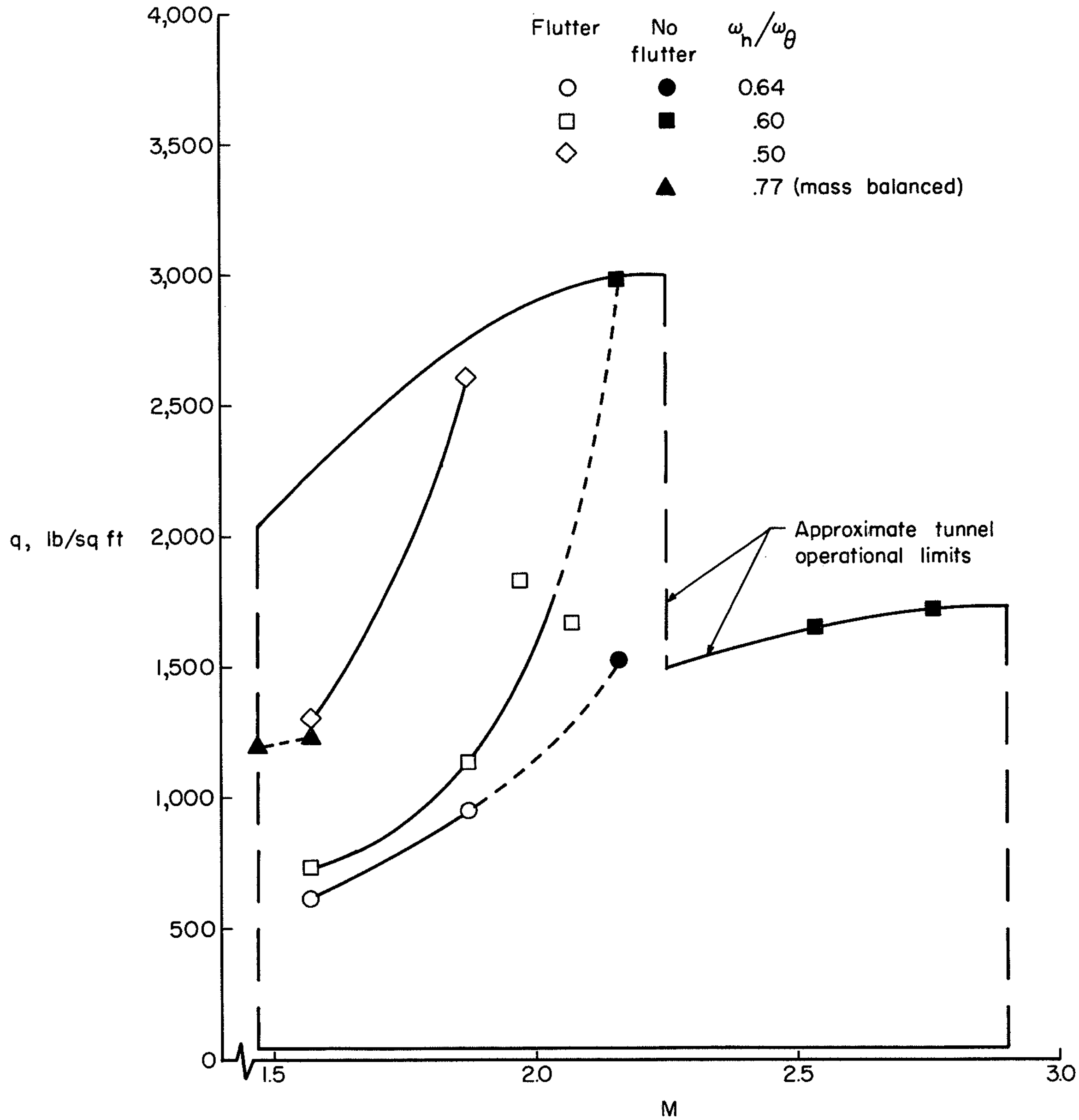

(c) Series 3.

Figure 3.- Continued.

[redacted]

[redacted]

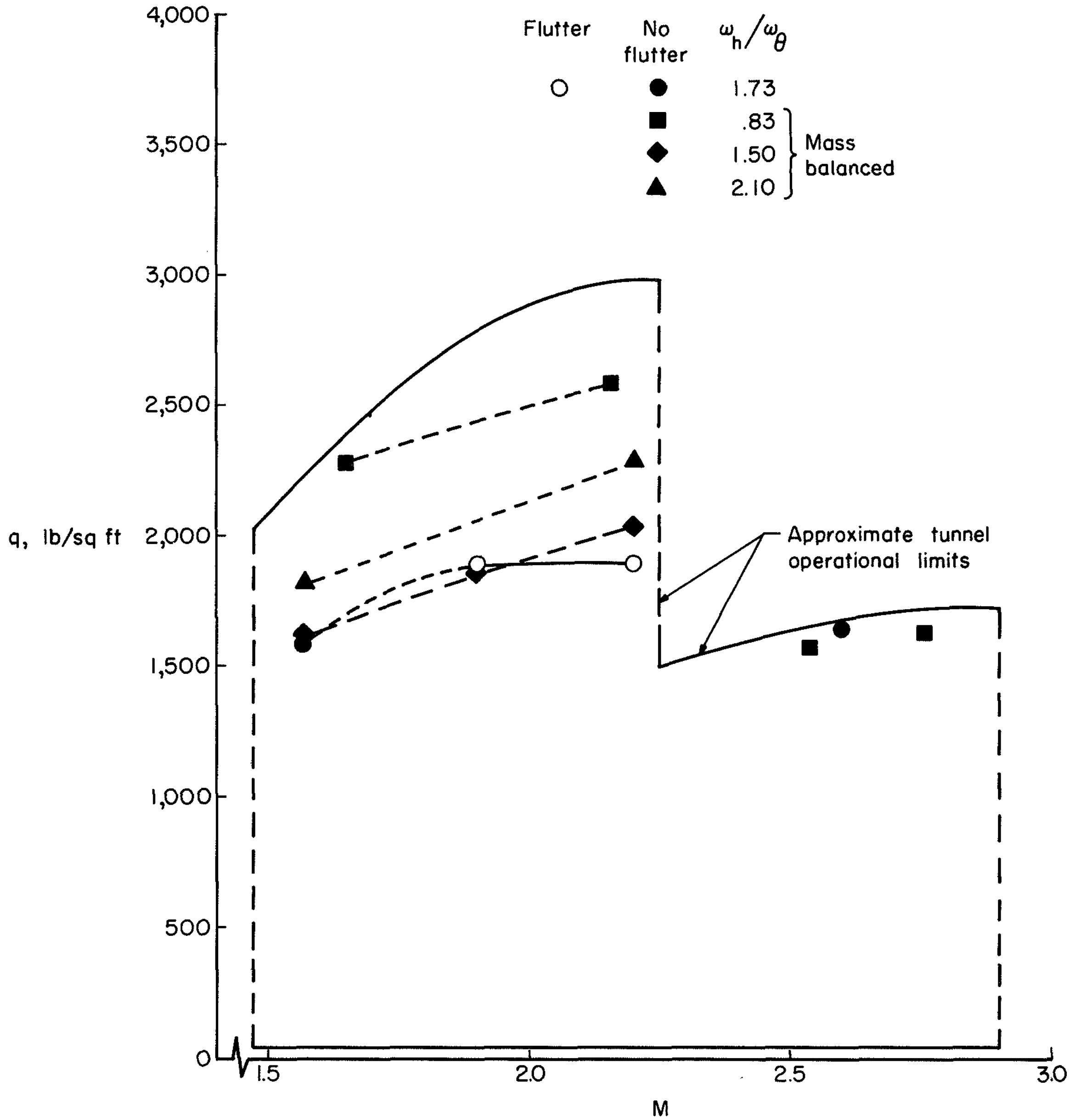

(d) Series 4.

Figure 3.- Concluded.

L-1261

[redacted]

L-1261

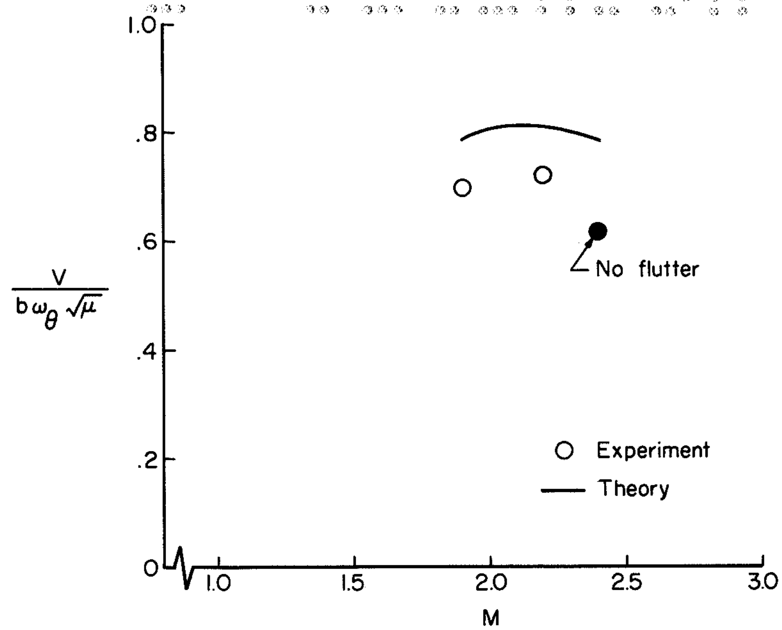

(a) $\frac{\omega_h}{\omega_\theta} = 0.59.$

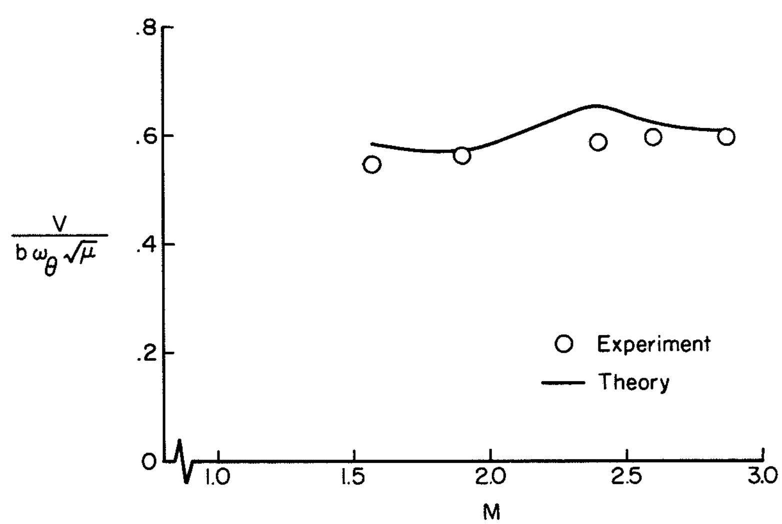

(b) $\frac{\omega_h}{\omega_\theta} \approx 0.72.$

Figure 4.- Comparison of variation of experimental and calculated velocity index parameter with Mach number for models of series 1.

[redacted]

[redacted]

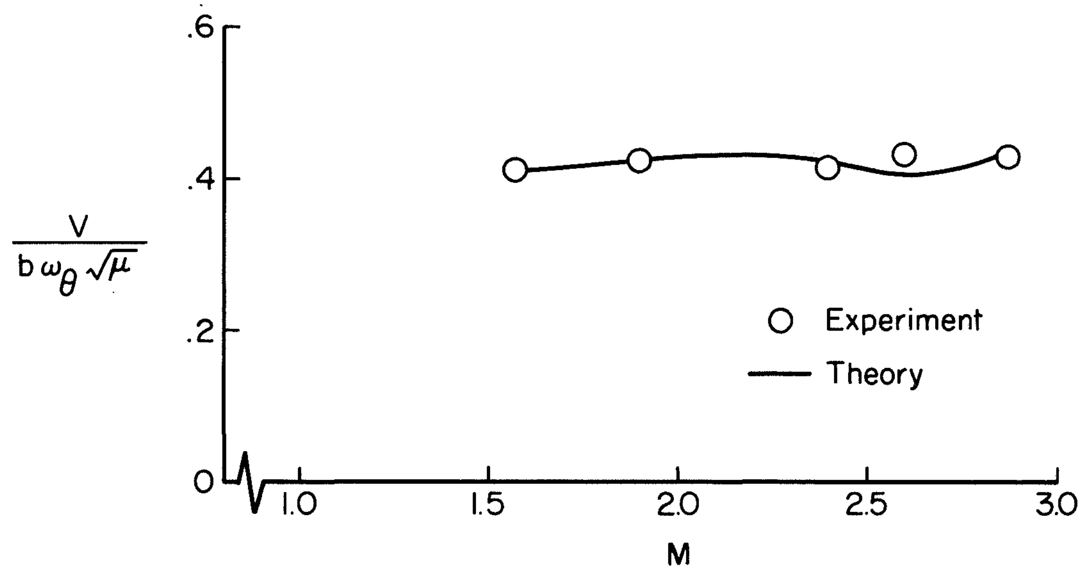

(c) $\frac{\omega_h}{\omega_\theta} \approx 0.96$.

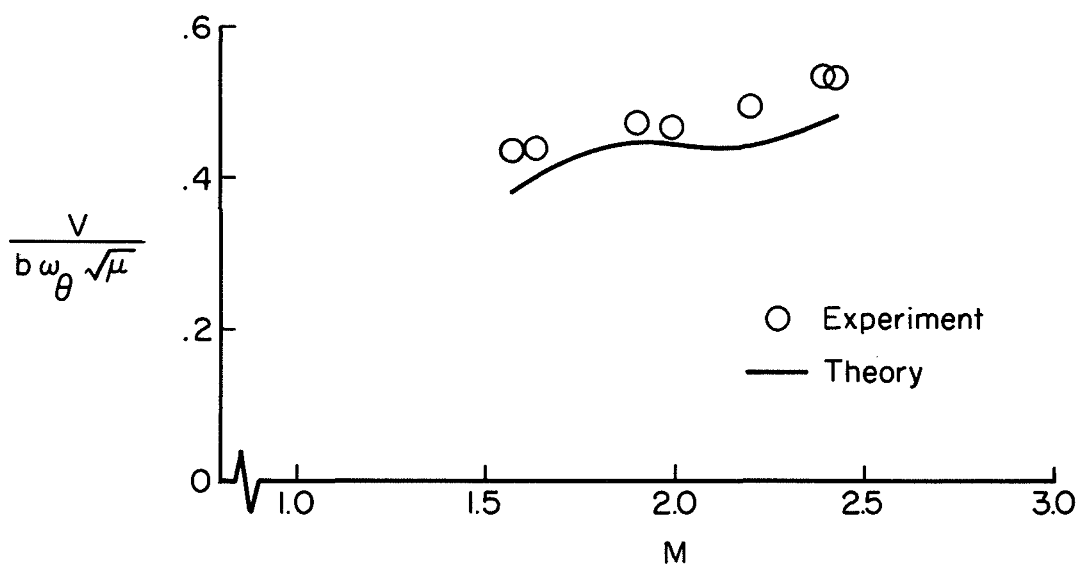

(d) $\frac{\omega_h}{\omega_\theta} \approx 0.93$ (mass balanced).

Figure 4.- Concluded.

L-1261

[redacted]

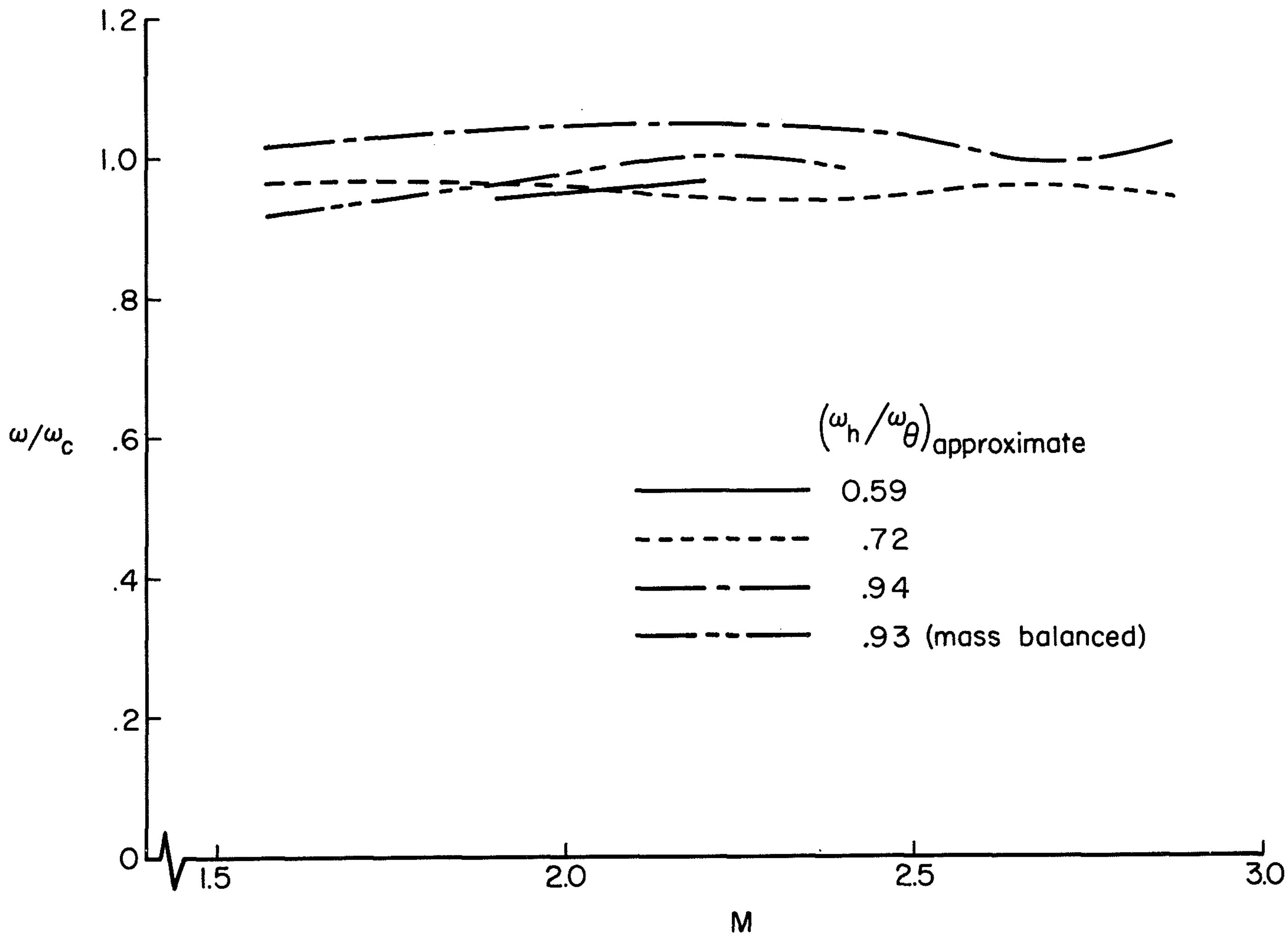

Figure 5.- Variation of ratio of experimental flutter frequency to calculated flutter frequency with Mach number for models of series 1.

[redacted]

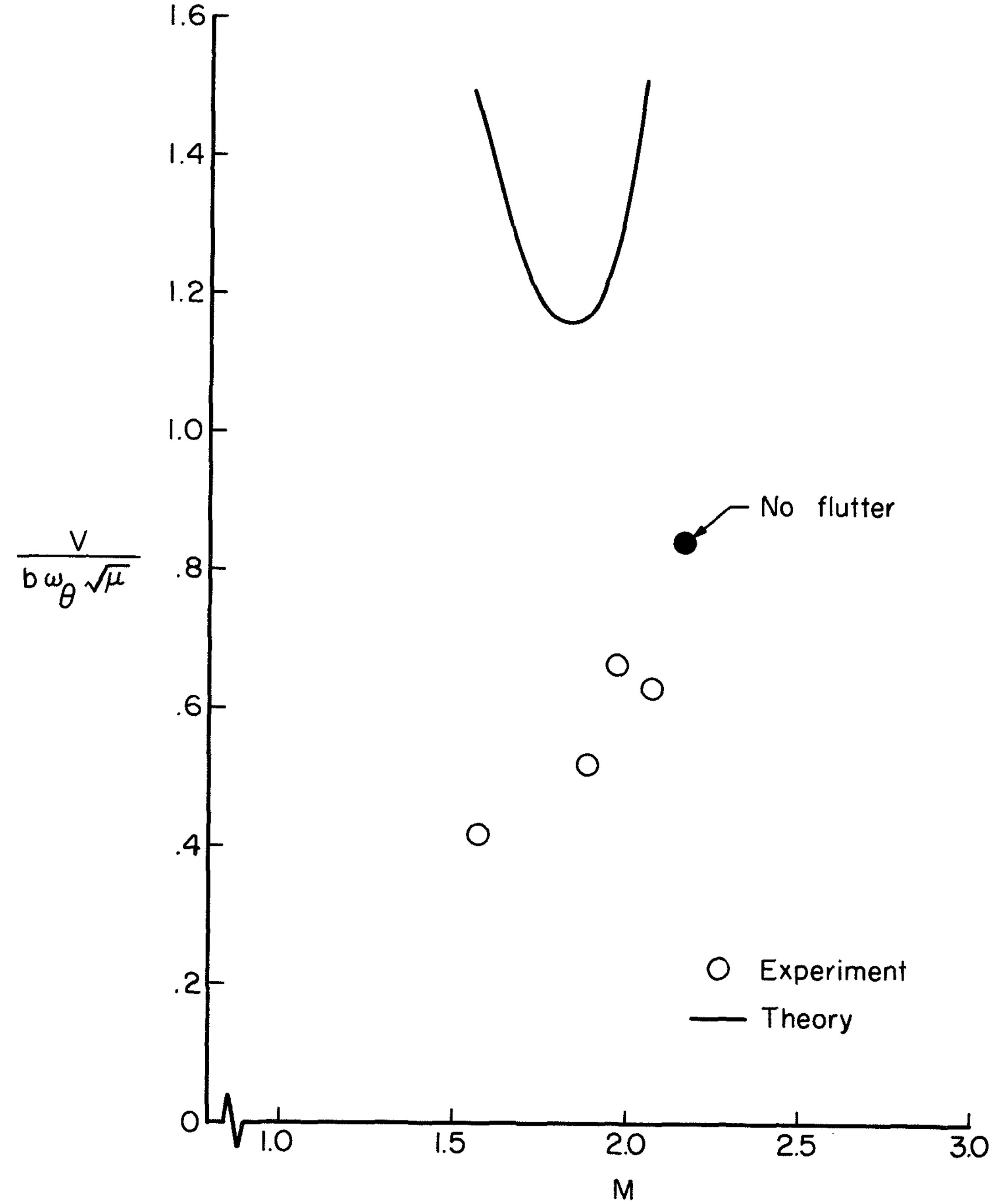

Figure 6.- Comparison of variation of experimental and calculated velocity index parameter with Mach number for model 3d. $\frac{\omega_h}{\omega_\theta} = 0.60$.

L-1261

[redacted]

[redacted]

[redacted]